THE BALTIC JOURNAL
OF ROAD AND BRIDGE ENGINEERING
2026/21(1)

ISSN 1822-427X/eISSN 1822-4288
2026 Volume 21 Issue 1: 1–23
https://doi.org/10.7250/bjrbe.2026-21.671

LOCAL BUCKLING ANALYSIS OF INNOVATIVE CORRUGATED PROFILE OF SOIL-STEEL COMPOSITE BRIDGES

NERIJUS BAREIKIS[1, *], ALGIRDAS JUOZAPAITIS[1], ILZE PAEGLĪTE[2]

[1]*Department of Steel and Composite Structures, Faculty of Civil Engineering, Vilnius Gediminas Technical University, Vilnius, Lithuania*

[2]*Department of Civil Engineering, Faculty of Civil and Mechanical Engineering, Riga Technical University, Riga, Latvia*

Received 20 October 2025; accepted 15 January 2026

Abstract. Corrugated soil-steel composite bridges due to their out-of-plane stiffness and interaction with surrounding soil are extensively used in the underground engineering. The demand for larger span of corrugated soil-steel structures is rising due to their high strength-to-cost ratio. Larger spans are usually related to the bigger cross-sections of corrugation profile. The use of the deepest corrugations like 500 mm pitch and 237 mm depth is associated with a higher risk of local buckling of straight region (tangent m_t) of corrugation. This study analyses the resistance to local buckling of four widely used corrugation profiles. It also examines the impact of circular hollow section steel pipes and high strength steel influence on plate width-to-thickness ratio limit. The numerical three-dimensional model was developed for the investigation. At first, parametric study was conducted to reveal the influence mechanisms on critical parameters, incorporating finite element mesh size, number of corrugations, plate height, and plate thickness. Afterwards, local buckling behaviour of corrugated steel plate was studied and width-to-thickness ratio

* Corresponding author. E-mail: nerijus.bareikis@vilniustech.lt

Nerijus BAREIKIS (ORCID ID 0009-0006-6744-0782)
Algirdas JUOZAPAITIS (ORCID ID 0000-0002-8067-6363)
Ilze PAEGLĪTE (ORCID ID 0000-0001-5810-2032)

limit was proposed considering that local buckling of the plate would not occur before steel yielding. It was found that corrugated plate thickness could be significantly reduced as a result of the reduction of buckling length by steel pipes. Therefore, innovative corrugation profile has the great potential to be rational more than the increase of the thickness of the regular corrugated steel plate.

Keywords: corrugated steel structure, corrugated profile, local buckling, parametric analysis, soil-steel composite bridge, strengthening techniques.

Introduction

Corrugated soil-steel (CSS) composite structures are already well known in the underground engineering due to their out-of-plane stiffness and high strength-to-cost ratio. CSS structures in the interaction with well compacted granular soil are recognised as composite structures, which can overtake various types of very heavy loads (Andersson & Karoumi, 2017; Beben, 2017; Nakhostin et al., 2021; Pettersson et al., 2015; Pettersson & Sundquist, 2014). Moreover, considering lightweight, quick installation process, lower environment impact and other advantages over traditional concrete girder bridges CSS structures are widely used in the culverts, bridges, tunnels, pedestrian and animal crossings, military applications, utility tunnels and civil engineering (Cirulis & Cirulis, 2017; Du et al., 2014; Elshimi et al., 2014; Jeon & Rigby, 2019; Mahgoub & El Naggar, 2021; Wang et al., 2018).

The demand of CSS composite structures is growing not only by their application, but also larger spans to cover larger clearance boxes are required by the market (Wadi et al., 2018, 2020; Wadi & Pettersson, 2017). Such adaptation to the needs is very well associated with the growth of the pitch and the depth of corrugation profile. Shallow corrugation profiles like 68×13 mm are widely used for the small starting from 300 mm diameter pipes. However, the deepest corrugation of 500 mm pitch and 237 mm depth allowed building the Guinness record world's largest span of 32.40 m (Embaby et al., 2022a). Larger spans usually require thicker plates, higher steel grades or bigger cross-sections of corrugation profile. Unfortunately, the use of the deepest corrugations leads to a higher risk to local buckling. To prevent local buckling by simply increasing plate thickness and setting minimal plate width-to-thickness ratio limit is commonly applied to the traditional steel girder structures according to Eurocode 3 (European Committee for Standardization, 2005). Such an approach and the influence on CSS composite structures are not deeply analysed and only few articles suggest the limitations (Chen et al., 2019; Cranston et al., 2016; Dou et al., 2016; Guo & Sause, 2014; Sun et al., 2023).

Chen et al. (2019) studied local buckling of the straight region of corrugation in a pipe-arch type of structures. The authors derived theoretical formulae for the elastic local buckling according to the Rayleigh-Ritz method and took the soil support into consideration. In addition, they modified the derived theoretical formulae according

to the results from finite element model (FEM) analysis and proposed a limit of the width-to-thickness ratio for the straight region of corrugation for pipe-arch type of structures. However, Chen et al. (2019) did not consider steel elastoplastic behaviour and initial imperfections in their study. Moreover, suggested limits were validated for pipe-arch structures only.

Sun et al. (2023) proposed width-to-thickness ratio limit to prevent local buckling and presented the strength design recommendations for the deeply buried circular corrugated steel arches with various rise-to-span ratios under axial compression and under combined axial compression and bending moment, respectively. They established FEM where they constrained the out-of-plane displacement at the crest and valley of corrugation and so eliminated other possible buckling modes except the local buckling under the axial compression only. Nevertheless, width-to-thickness ratio limit proposed by Sun et al. (2023) did not cover the deepest corrugation profile of 500×237 mm. Moreover, as results in this article show, defining only one limiting value for shallow and the deepest corrugation profiles could be very conservative considering that the local buckling of shallow corrugation profiles occurs after steel yielding.

Piekarczuk et al. (2015), in their experimental and numerical study of profiled steel sheets used for self-supporting arch structures, highlighted the necessity to consider imperfections and other disturbances of the shape during the FEM modelling. Otherwise, it leads to highly overestimated value of critical buckling load and displacements. Piekarczuk et al. (2015) used the 3D digital image correlation (DIC) method for the purpose of measurement of displacement and strain fields during the experiment. Later, these results were used to validate arch section numerical models as DIC gave reliable information about the actual buckling modes. DIC method could be also applied for any other types of corrugation profiles to determine the level of imperfections. However, representation of the real imperfections in FE models is still very time consuming and demanding for computing power.

Furthermore, a detailed investigation is necessary for the use of circular hollow section steel pipes and the influence of high-strength steel (HSS) on the local buckling of regular corrugation. Investigation results presented by Bareikis (2024a) show the potential of cross-section area reduction by the implementation of circular steel pipes. Moreover, it was concluded that strengthening corrugated steel plates with circular steel pipes will allow for the control of local buckling of the straight region (tangent m_t) of corrugation; however, a deeper analysis was requested. Additionally, circular steel pipes could be rationally utilised as an alternative method of already proposed strengthening techniques to increase the bearing capacity of CSS structures (Bareikis, 2024b; Beben & Manko, 2010; Beben & Stryczek, 2016; Embaby et al., 2022b; Maleska & Beben, 2019; Wysokowski, 2021). Bareikis's (2025) study of HSS influence on the utilisation ratio of large

span CSS structures indicated 32.7% utilisation ratio reduction in transition from conventional 420 MPa steel to high strength of 690 MPa steel for 17.5 m span open two-radius arch profile. However, the use of higher steel grades is directly associated with lower resistance to local buckling due to higher yielding, and it must also be investigated.

In the current study, the resistance to local buckling of four typical and widely used regular corrugation profiles was analysed. In addition, this study investigated the impact of innovative corrugation cross-section strengthened with circular hollow section steel pipes and HSS influence on minimal plate width-to-thickness ratio limit. Cross-sections of regular and innovative corrugation profiles are shown in Figure 1. Despite that corrugation straight region (tangent m_t) length slightly depends on the plate thickness, it was decided to study only axial tangent length behaviour.

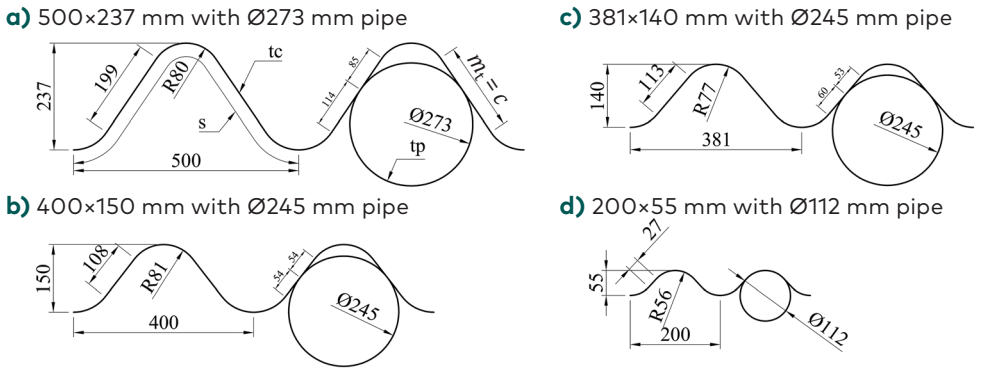

Figure 1. Cross-sections of regular and innovative corrugation profiles with circular pipes

In the beginning, the numerical 3D model was developed and the parametric study was conducted. The main objective of parametric study was to define critical parameters which have influence on critical buckling load: finite element mesh size; number of corrugations; plate height and plate thickness. Secondly, local buckling behaviour of corrugated steel plate was studied. Width-to-thickness ratio limit under axial compression was determined under the assumption that steel plate critical buckling stresses should be always above a steel yielding point to prevent local buckling.

1. Local buckling analysis

1.1. Finite element model and size range of CSS

For the investigation of regular and innovative corrugation resistance to local buckling, a three-dimensional nonlinear FE model was developed with the use of COMSOL Multiphysics (2024). To create the model, it was decided to generate a full corrugation profile without any restrictions on the shape and direction of buckling, as shown in Figure 2 (Bi & Yang, 2024).

a) a meshed regular corrugation profile of 381×140 mm

b) a meshed innovative corrugation profile of 381×140 mm with Ø245 mm circular hollow section steel pipes in each wave

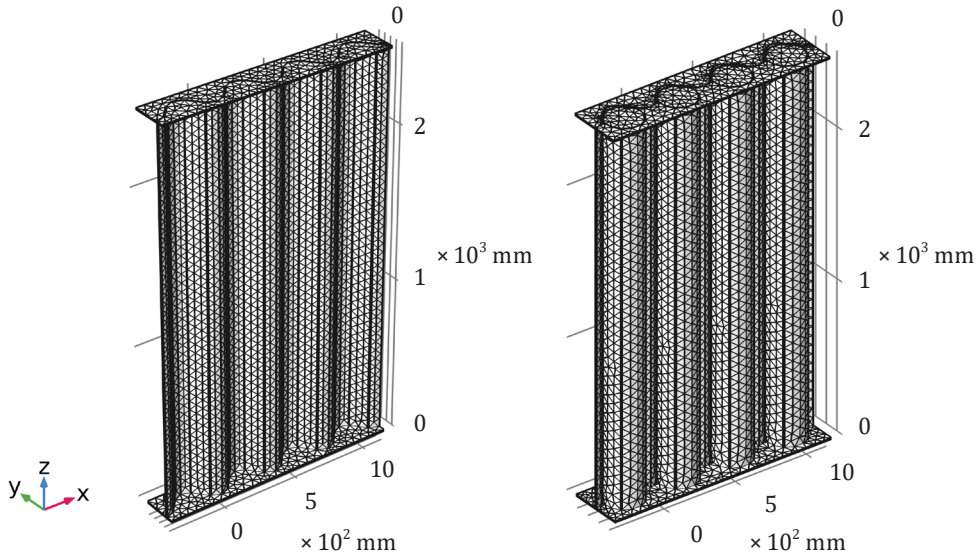

Figure 2. FE model for local buckling investigation

Straight (not curved) corrugated plate parallel to *z* axis was modelled in the software with top and bottom base plates replicating the sample of potential experimental study. Corrugated plates and base plates were modelled as *shell* elements. Mesh type of *free triangular* was selected to create an unstructured triangular mesh on shell elements. Base plates dimensions: length was set to be equal to corrugated plate width; width was 100 mm wider than corrugated plate depth or the depth of innovative corrugation profile; thickness – 50 mm. Constraint

of *symmetry* was applied for corrugated plate free edges and base plates edges in *x* direction. Top and bottom base plate edges in *y* direction were set to be *free*, and this was the reason for the flexural buckling mode (see Figure 3). Bottom base plate was pinned to restrict movements in *x*, *y*, and *z* direction. The corresponding steel parameters assumed in the model: Young's modulus $E = 2.00 \times 10^5$ MPa, Poisson's ratio $\nu = 0.3$, density 7850 kg/m^3.

According to COMSOL Multiphysics (2024) documentation, a linearized buckling analysis can be used to estimate the critical load at which a structure becomes unstable. This is a predefined study type that consists of two study steps: an initial step in which a unit load is applied to the structure and the second step in which an eigenvalue problem is solved for the critical buckling load. COMSOL reports a critical load factor, which is the value of load multiplier λ at which the structure becomes unstable. The level of the initial load used is immaterial since a linear problem is solved. If the initial load was larger than the buckling load, then the critical value of λ is smaller than 1. Considering this feature, to get a critical load factor at which corrugated plate becomes unstable, the top surface area of top base plate was loaded by concentrated load of –1.0 kN initiating axial compression parallel to *z* direction. When necessary, the load and the results can be converted to kN/m or to kN/m^2 according to top base plate dimensions.

The corresponding deformation that is reported by COMSOL is the shape of the structure in its buckled state. Small deviations from the theoretical geometrical shape can then have a large impact on the actual buckling load. To include the impact of potential geometric imperfections into the model, the prescribed deformation of the magnitude of $m_t/200$ was applied to the tangent of corrugation. Also, it was decided to move top base plate by 5 mm in $-x$ and y direction considering it as geometric fabrication tolerance.

It should be noted that linearized buckling analysis was validated on fundamental FE models (Benchmark Tests): long slender pinnedend column buckling and long thin plate buckling analysis. Both tests predicted accurate results of corresponding buckled shape, critical Euler load and stress. Nevertheless, to eliminate geometric variability, it is planned to calibrate FE models and to adjust presented results using future experimental data. However, laboratory test is not in the scope of this article, but it is already planned for future work.

Decision to model a full corrugation profile without restriction of top base plate movement to *y* direction allowed registering not only critical buckling load factor values but also specific buckling shapes for each specimen. Even though in some of the cases, the first buckling mode was identified as flexural buckling, only the first buckling shape of local buckling and the critical load factor from local buckling were further studied in this article. In general, during the analysis, three different buckling shapes were recognised: flexural buckling, plate local buckling and pipe local buckling (see Figure 3).

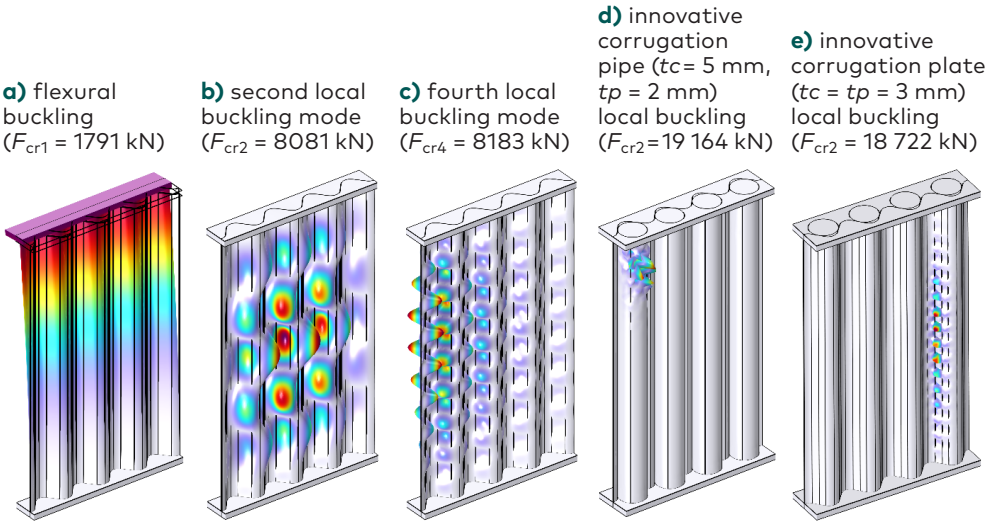

Figure 3. Buckling modes for 381×140 mm corrugation profile of tc = 5 mm and H = 2.5 m

As can be seen in Figure 3, the tangent of corrugation m_t is always less resistant to deformation than the crest or valley of corrugation. Unfortunately, in practice, it is not possible to produce only the tangent of corrugation from thicker steel because of the nature of the production processes of such sinusoidal corrugations. Therefore, to prevent local buckling, the whole cross-section of the corrugation profile must be designed thicker. Such a disadvantage was one of the main key factors in the introduction of circular steel pipes with the expectation of reducing the tangent length (buckling length) of corrugation. Moreover, as later results will show, the introduction of steel pipes allowed the same stiffness of a plate with lower consumption of steel (lower cross-section area).

As presented in Figure 1, the outside diameters of circular pipes were selected in a way that the corrugated plate tangent must be divided into two as close as possible, similar parts. A steel pipe with a diameter of 245 mm perfectly fits the 400×150 mm corrugation profile. The same diameter pipe was also selected for the 381×140 mm corrugation plate; however, the straight part of the corrugation was not equally divided. The same can be seen for a 500×237 mm corrugation, as the OD273 mm pipe reduced the buckling length to 114 mm (longer part). For a shallow corrugation profile of 200 mm pitch and 55 mm depth, the OD112 mm pipe fits precisely to the crest of the corrugation. As later results show, such shallow corrugation profiles with short tangent lengths will not fail due to local buckling. It

must be noted that a fixed connection between the corrugated plate and the circular hollow section steel pipe was assumed in this article. Also, the effect of soil support on the local buckling of corrugation under axial compression is minimal and can be neglected (Cranston et al., 2016).

1.2. Elastic buckling behaviour and parameters analysis

When FE models, according to Section 1.1, were ready for the linearized buckling analysis, it was necessary to run a sensitivity to critical buckling load study on finite element mesh size, number of corrugations, plate height, and plate thickness. Following classical thin plate buckling theory, the elastic local buckling stress of the corrugated plate can be calculated according to Equation (1) (Sun et al., 2023):

$$\sigma_{cr} = \frac{F_{cr}}{n_s st}, \tag{1}$$

where F_{cr} – critical buckling load obtained from a finite element analysis (FEA), n_s – number of waves, s – expansion length of one repeating corrugation section (see Figure 1), t – corrugated steel plate thickness.

Then, buckling coefficient k_{Lc} can be expressed by Equation (2) that allows presenting critical buckling load sensitivity results on analysed parameters (Sun et al., 2023):

$$k_{Lc} = \frac{F_{cr} 12\left(1-\nu^2\right)\beta^2}{n_s st \pi^2 E} \tag{2}$$

where ν – steel Poisson ratio (ν = 0.3), β – width-to-thickness ratio ($\beta = s/2t$), E – steel Young's modulus $E = 2.00\times10^5$ MPa.

A denser FE mesh generally improves simulation accuracy and can lead to closer agreement with experimental data by better capturing the geometry and stress variations. However, increasing mesh density is not always a guarantee for more accurate results due to several issues like stress concentration, computational cost, or convergence issues. No matter how fine the mesh, inaccuracies in material properties, boundary conditions, or modelling assumptions can dominate the results. Extremely dense meshes may model numerical noise rather than meaningful physical stress variations. In light of the above, it was decided to run a mesh convergence study to ensure the results are stable without unnecessary computational expense. Buckling coefficient results of the mesh convergence study are presented in Figure 4. Notable, that the *Normal* and more dense FE mesh does not increase the accuracy of buckling coefficient results for all four types of corrugation profiles analysed in this article. For further analysis, the FE mesh was

set to *Normal*. Max and min finite element size, also boundary and edge elements of the complete mesh of the model, according to a predefined name for a regular 381×140 mm corrugation profile, are presented in Table 1.

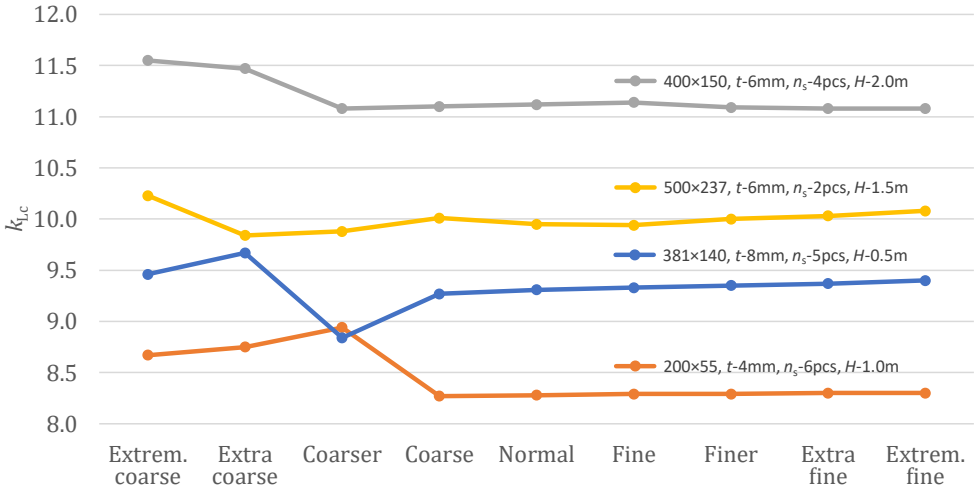

Figure 4. Buckling coefficient results for the FE mesh density

Table 1. The size and number of finite elements according to predefined name for regular 381×140 mm corrugation profile, n_s = 4, H = 2.5 m

Predefined name	Maximum FE size, mm	Minimum FE size, mm	Boundary elements of complete mesh	Edge elements of complete mesh
Extremely coarse	1250	175	848	459
Extra coarse	750	135	1059	568
Coarser	475	100	1763	731
Coarse	375	70	3694	1042
Normal	250	45	6669	1544
Fine	200	25	8261	1846
Finer	138	10	13636	2269
Extra fine	87.5	3.75	23200	3035
Extremely fine	50	0.50	44648	4521

The number of waves n_s influences accuracy results of buckling coefficient k_{Lc}, as shown in Figure 5. It is worth noting that other parameters such as plate thickness,

plate length, and mesh density are different for each corrugation profile. It was done to provoke different behaviour on buckling coefficient results, and it is well seen for 500×237 mm corrugation profile where k_{Lc} dependency on n_s is almost linear. Nevertheless, more than four waves of corrugation do not have significant influence on the results, so n_s = 4 was applied for the remaining analysis.

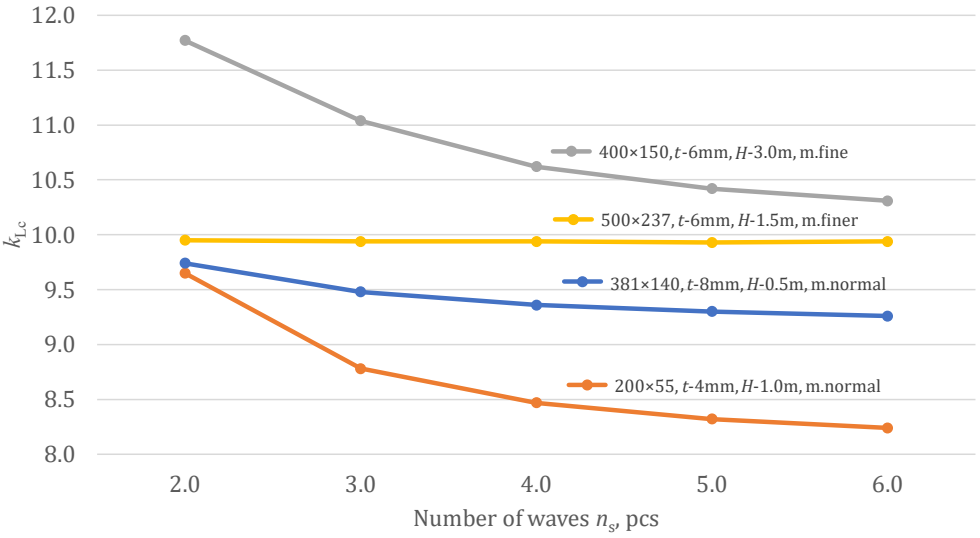

Figure 5. Buckling coefficient results for the number of waves n_s

The influence of corrugated plate height (H) on the buckling coefficient was also investigated (see Figure 6). Considering FE model constraint conditions, plate height is directly associated with buckling shape, which is always identified as flexural buckling for higher FE models, so the influence of plate height on k_{Lc} can be ignored approximately. However, results presented in Figure 6 are collected from the buckling shape of local buckling only. Nevertheless, a plate higher than 2.5 m does not present more sensitive buckling coefficient results, so H = 2.5 m was chosen for the following result comparison.

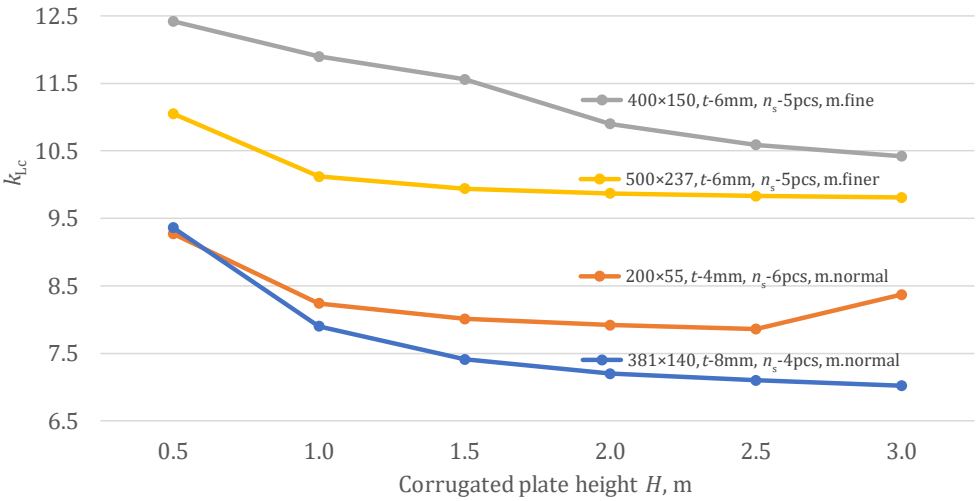

Figure 6. Buckling coefficient results for the height of the corrugated plate H

Buckling coefficient dependency on corrugated plate thickness (t) under axial compression is reflected in Figure 7. Obviously, k_{Lc} decreases when plate thickness becomes thicker, and such decreasing behaviour is obtained for all investigated corrugation profiles. In addition, Figure 8 represents the plate thickness nonlinear influence on critical buckling load F_{cr} and the results in this case can be comparable. A higher critical buckling load is necessary to arouse local buckling when the plate thickness increases. Moreover, corrugation profiles with smaller wave dimensions tend to be more resistant to local buckling because of a shorter straight region of corrugation. However, it is not the case for the 381×140 mm corrugation profile, due to the longer tangent (see Figure 1), and naturally it is less resistant to local buckling than the 400×150 mm corrugation profile.

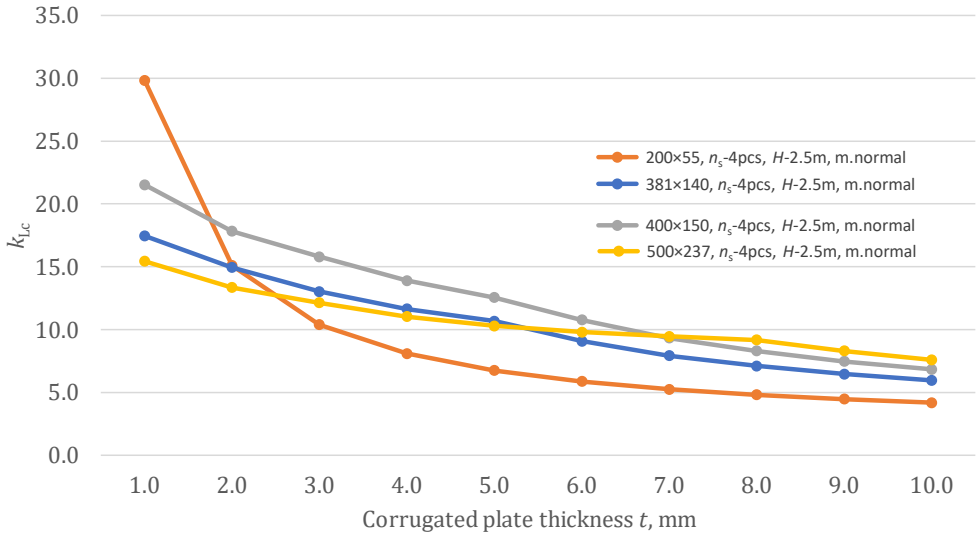

Figure 7. Buckling coefficient results for the thickness of the corrugated plate t

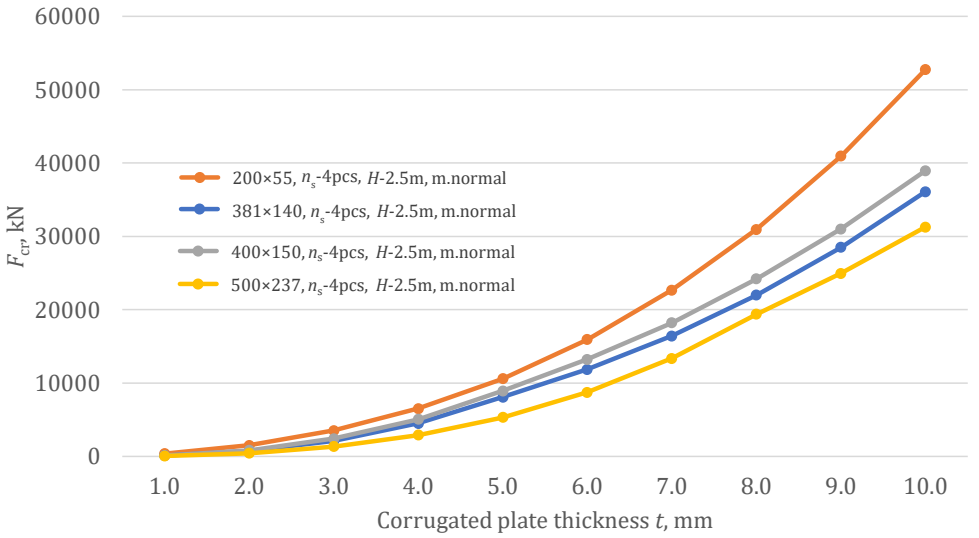

Figure 8. Critical buckling load results for the thickness of the corrugated plate t

Also, specific deviations from nonlinear curves could be noticed in Figure 7. It was found that it was related to the change of local buckling shape from (*c*) to (*b*)

as presented in Figure 3. For example, (*c*) type buckling mode was identified for 381×140 mm and 400×150 mm corrugation profiles up to 5 mm thick plate and it changed to (*b*) type local buckling for thicker plates. Same behaviour was obtained for 500×237 mm corrugation when (*b*) buckling shape was registered for 9 mm and thicker plates. Local buckling in the shape of (*b*) was always the case for 200×55 mm corrugation.

The findings suggest that corrugation profiles with tangent of 27 mm or shorter will not fail because of local buckling under axial compression. For example, critical buckling stresses of FE model of 200×55 mm corrugation and even 1.0 mm thick plate are equal to 400 MPa. In practical engineering, such value will be above the limit of yielding stress because usually S355 or lower steel grades and thicker plates are utilised for shallow corrugations.

1.3. Width-to-thickness ratio under axial compression

To present the results, it was decided to calculate normalized width-to-thickness ratio λ_n and local buckling stability coefficient φ_c under axial compression according to Equations (3) and (4) and later to plot their relationship (Sun et al., 2023).

$$\lambda_n = \sqrt{\frac{f_y}{\sigma_{cr}}} \leq 1.0 \tag{3}$$

$$\varphi_c = \frac{\sigma_{cr}}{f_y} \tag{4}$$

Relationship results of all regular corrugation profiles investigated in this article are plotted in Figure 9. To prevent local buckling of straight region of corrugation before yielding, it was assumed that a normalized width-to-thickness ratio cannot be higher than 1.0. Meanwhile, stability coefficient values higher than 1.0 were set to be equal to one just for better visualisation of the results. Figure 9 demonstrates the results of four in practice used and one theoretical steel grade (355; 420; 500; 690, and 1300 MPa).

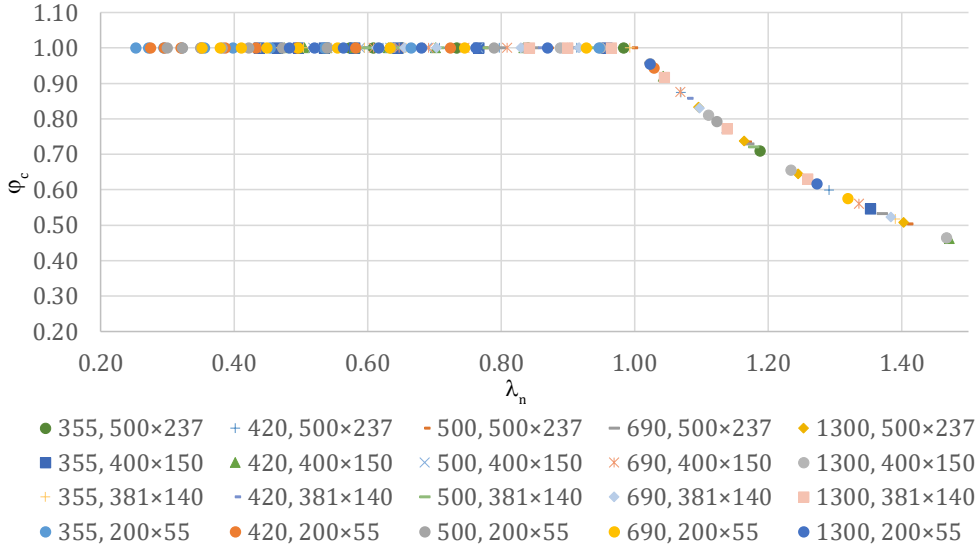

Figure 9. Width-to-thickness ratio λ_n results for all investigated corrugation profiles

Results of a minimal plate resistant to local buckling for each investigated corrugation profile are shown in Figures 10 and 11. Plate of thickness indicated on the left side of the red line ($\lambda_n \leq 1.0$) is assumed to be safe against local buckling of straight region of corrugation under axial compression. The thickness of the corrugated plate defined in rectangles was set from 1 mm to 10 mm accordingly. To prevent local buckling deeper corrugations with longer tangent requests thicker plates while shallow corrugations like 200×55 mm fails only at higher steel grades and when plate thickness is unrealistically low.

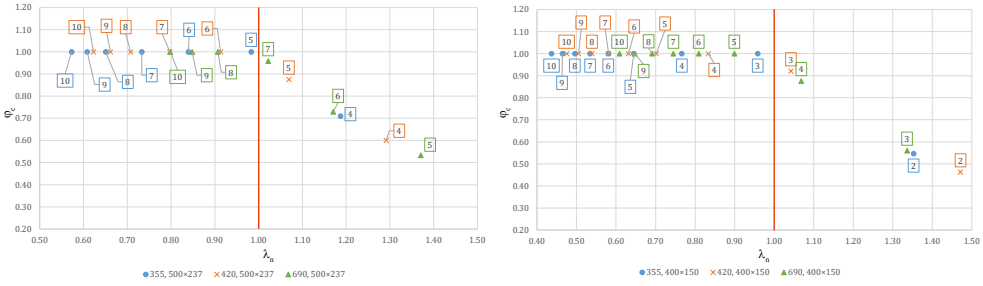

Figure 10. λ_n results for 500×237 mm and 400×150 mm corrugation profiles

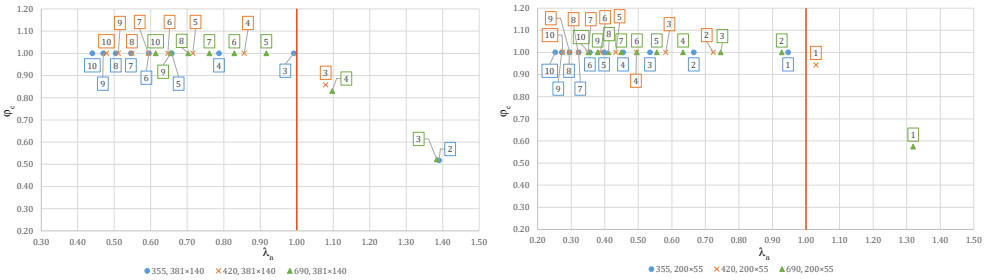

Figure 11. λ_n results for 381×140 mm and 200×55 mm corrugation profiles

Figure 12 contains width-to-thickness ratio results of innovative corrugation profiles: 500×237 mm each wave of corrugation reinforced by circular hollow section steel pipes OD237 mm and 381×140 mm reinforced by OD245 mm steel pipes.

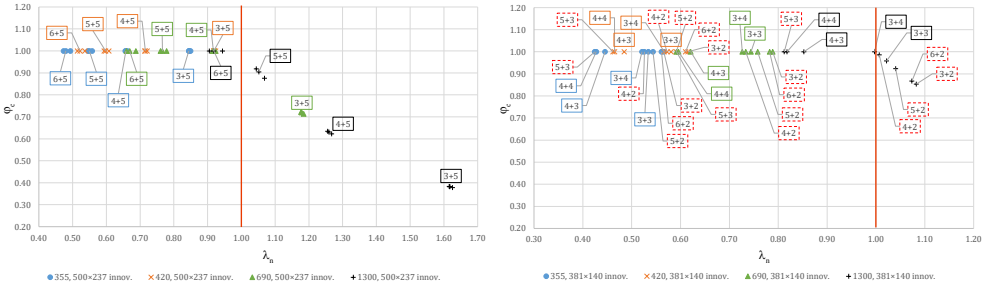

Figure 12. λ_n results for innovative 500×237 mm and 381×140 mm corrugation profiles

The combinations of corrugated plate and pipe wall thickness were chosen based on the nearby cross-section area values of regular and innovative corrugation profiles. The first number in rectangles represents corrugated plate thickness and the second number – pipe wall thickness. Moreover, results in red dashed rectangles indicate evidence of local buckling in pipe wall only (see Figure 3). Pipe local buckling for 500×237 mm corrugation profile was recorded only in the combination of 6+4 mm. In addition, it could be noticed that width-to-thickness ratio results for 500×237 mm corrugation profile are concentrated by small groups, for example, one group of 6+4, 6+5 and 6+6 mm. The reason of such concentration could be explained as follows: by the increase of pipe wall thickness the resistance to critical buckling load and cross-section area also increase so that, finally, critical stresses do not fluctuate much. It could be concluded that under axial compression pipe wall thickness has minor effect on corrugated plate tangent buckling. However, pipes

existence shortens buckling length of straight region of corrugation allowing one to utilise thinner corrugated plates, and the following results will confirm that the cross-section area of innovative corrugated profiles remains competitive.

Pipe local buckling is much more common for 381×140 mm innovative corrugation profile where lower pipe wall thickness was applied (see Figure 12). Because of the same reason, the results are much more scattered. Nevertheless, it was found that pipe started to buckle first when its wall thickness was by two or more millimetres thinner than that of the corrugated plate. However, such a relationship and synergistic failure mechanism between the steel pipe and the corrugated plate should be investigated more in the future to ensure that pipe local buckling is always prevented, and it is beyond the scope of this article. Omitting the pipe buckling results, the remaining are arranged sequentially from left to right in the direction of decreasing cross-sectional area, the same for the 500×237 mm and 381×140 mm corrugation profiles. The tendency of the results for the 400×150 mm corrugation profile is almost the same as for 381×140 mm. Additionally, as shown in previous results, tangent local buckling of 200×55 mm corrugation profile could be questionable only when very low, unrealistic and usually not applicable in practice plate thickness is applied. Considering that, results for 400×150 and 200×55 are not presented.

Calculation of normalized width-to-thickness ratio λ_n is not something very convenient because critical stress or critical buckling factor must be determined numerically. Therefore, it was decided to propose a ratio limit value of tangent length to corrugated plate thickness c/t ($c = m_t$, see Figure 1). Such an approach is commonly applied during the design of regular steel girder structures according to Eurocode 3 regulations (European Committee for Standardization, 2005). Furthermore, Eurocode 3 (European Committee for Standardization, 2005) is not adopted specifically for the corrugated soil-steel composite structures, so it was necessary to understand and to compare the proposed c/t ratio limiting values. Dependency of c/t ratio on yield strength of steel for specific regular corrugation profiles is indicated in Figure 13, and the results of few innovative corrugation profiles are presented in Figure 14, respectively. The results of maximum width-to-thickness ratios for parts subjected to compression are summarized and listed in Table 2.

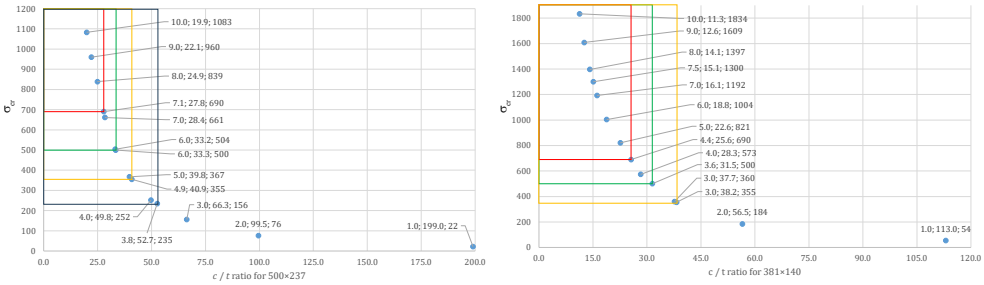

Figure 13. *c/t* ratios for regular 500×237 mm and 381×140 mm corrugation profiles

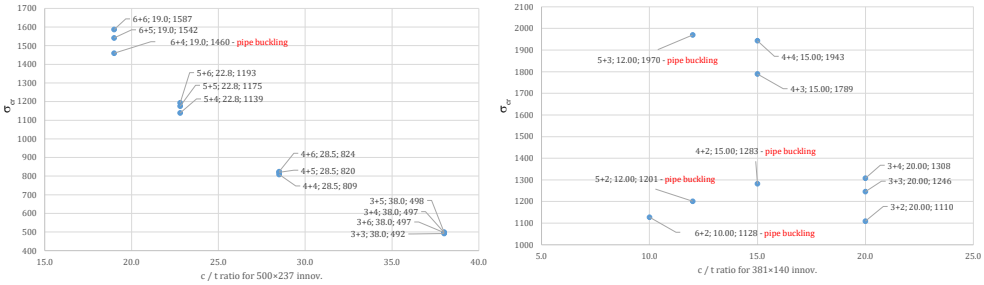

Figure 14. *c/t* ratios for innovative 500×237 mm and 381×140 mm corrugation profiles

Table 2. Proposed *c/t* and *s/2t* ratio limiting values

Corrugation profile, mm	*c/t*	*s/2t*
500×237	$\leq 47\varepsilon_k$	$\leq 86\varepsilon_k$
400×150	$\leq 42\varepsilon_k$	$\leq 100\varepsilon_k$
381×140	$\leq 43\varepsilon_k$	$\leq 92\varepsilon_k$
200×55	$\leq 25\varepsilon_k$	$\leq 110\varepsilon_k$
500×237 innovative	$\leq 53\varepsilon_k$	$\leq 93\varepsilon_k$
381×140 innovative	$\leq 44\varepsilon_k$	$\leq 92\varepsilon_k$

Note: $\varepsilon_k = \sqrt{235 / f_y}$.

Despite the values proposed in Table 2, to ensure resistance to local buckling, it is believed that the *c/t* ratio should be equal to or not greater than $42\varepsilon_k$, which for some corrugation profiles could be considered conservative. Nevertheless, it is reasonable with respect to Eurocode 3 (European Committee for Standardization, 2005), which proposes exactly the same limit for sections in class 3 under axial compression.

Class 3 cross-sections are those in which the stress in the extreme compression fibre of the steel member, assuming an elastic distribution of stresses, can reach the yield strength, but local buckling is liable to prevent development of the plastic moment resistance.

Sun et al. (2023) also investigated and proposed limit values for the width-to-thickness ratio β. However, β is a ratio of half of expansion length of one repeating corrugation section to corrugated plate thickness. It is important to highlight that expansion length *s* includes not only straight region of corrugation, but also half of the crest and half of the valley of corrugation, so comparison of the results with Eurocode 3 (European Committee for Standardization, 2005) is questionable. In addition, this study clearly indicated that according to numerical models prepared by COMSOL Multiphysics (2024) local buckling always starts on the tangent of corrugation. Nevertheless, β ratio limit values were also defined in this article, and they are listed in Table 2. The obtained ratios are closer to the study by Chen et al. (2019) than that proposed by Sun et al. (2023) and it could be related to the fact that critical buckling load was determined by the model of a full corrugation profile and not only of straight region of corrugation (see Figure 2).

1.4. Relationship of cross-section area and section modulus

According to the presented results, local buckling of the corrugation profile is associated with a longer straight region of corrugation, and obviously, buckling resistance is lower for thinner plates. Contrary to regular steel girder structures, it is not feasible to manufacture a corrugated plate with just a thicker tangent following standard production processes (plate corrugation and rolling). In order to prevent local buckling, plate thickness should be increased for a full corrugation profile (tangent, crest, and valley). As examined in this research, to prevent local buckling, thicker plates are also necessary when the higher yield strength steel is applied.

By the introduction of innovative corrugation cross-section strengthened with circular hollow section steel pipes, it was found that corrugated plate thickness could be significantly reduced because of the reduction of tangent length (buckling length). However, corrugation reinforcement by steel pipes also increases cross-section area, so it was important to investigate and answer the question – can innovative corrugation profile be considered a rational option? Therefore, it was decided to present the relationship between cross-section area A and section modulus W for the regular and innovative corrugation profiles studied in this article (see Figure 15). Results are based on cross-section parameters determined by SolidWorks Corporation (2024).

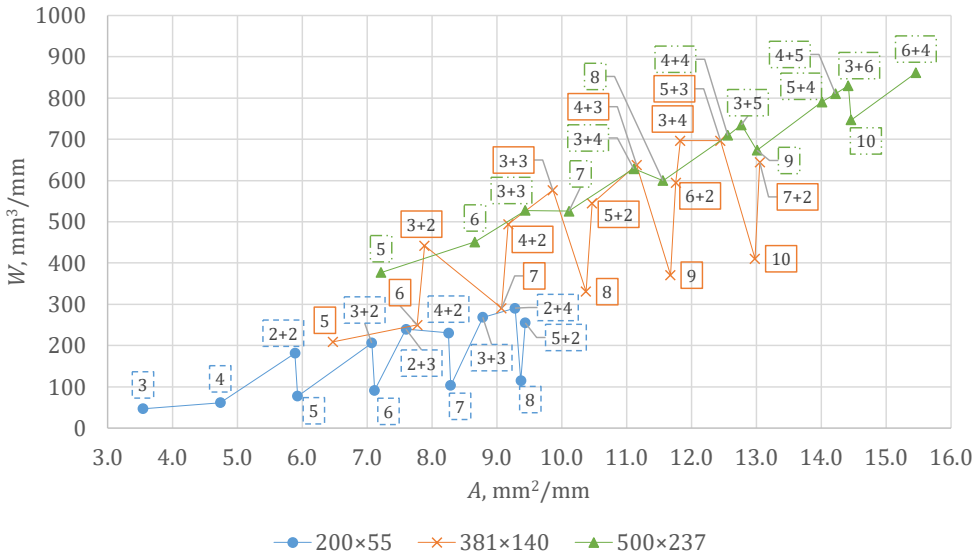

Figure 15. Relationship of cross-section area *A* and section modulus *W* of regular and innovative corrugation profiles

According to the presented results in Figure 15, the advantage of introduction of steel pipes is clearly visible. For example, the cross-section area for a 3+3 mm combination of 381×140 mm profile with steel pipes is more than 31% lower than for a regular 10 mm plate, while the section modulus is more than 40% higher. Even though critical buckling load for an innovative profile is lower, it is still safe against local buckling. By a lower percentage, but still an advantage is obtained for the 500×237 mm corrugation profile, where *A* for the 4+4 mm combination is about 3.5% lower than the regular 9 mm corrugated plate, while *W* is about 5.3% higher. For shallow 200×55 mm corrugation profile, *A* is lower by 59% and *W* is higher by 58% for the 2+2 mm innovative profile compared to the regular 8 mm plate. Corrugated plate reinforcement by steel pipes can increase the stiffness and overall bearing capacity of corrugation when the thickest plate, which could be corrugated and rolled, is not sufficient.

Conclusions

The paper investigated the resistance to local buckling of four widely used corrugation profiles. The analysis was conducted to assess the impact of circular hollow section steel pipes and HSS influence on the minimal plate

width-to-thickness ratio limit. The numerical 3D nonlinear model was developed to determine critical buckling factors, which were necessary for further analysis. Local buckling behaviour of corrugated steel plates was studied under axial compression, and width-to-thickness ratio limits were proposed to ensure the tangent of corrugation local buckling resistance prior to yielding. Conclusions of the investigation are listed below.

- An innovative corrugation cross-section strengthened with circular hollow section steel pipes was proposed for corrugated soil-steel composite structures. The numerical three-dimensional model was developed to investigate the influence of steel pipes on the local buckling of regular corrugation. Numerical results show that pipes increase corrugated plate local buckling critical stresses; therefore, a thinner corrugated plate can be applied (see Figures 13 and 14).
- The study additionally revealed that steel pipe started to buckle first when its wall thickness was by two or more millimetres thinner than that of the corrugated plate. However, in this article the relationship and interaction between the steel pipe and the corrugated plate was not investigated in detail but it is already planned in future work.
- To prevent local buckling before yielding width-to-thickness ratio limit was proposed for the regular corrugation and for the innovative corrugation strengthened with circular hollow section steel pipes cross-section. For some corrugations such a limit could be considered conservative; it is reasonable with respect to Eurocode 3 (European Committee for Standardization, 2005) which indicates the same limit for class 3 steel sections under axial compression.
- The introduction of an innovative corrugated cross-section, reinforced with steel pipes, is expected to result in an increase in the cross-sectional area. Therefore, the rationality of this innovative corrugated profile was investigated according to the mass (cross-sectional area) criterion. It was observed that regular corrugation plate thickness can be reduced by 30–50% because of introduction of steel pipes at the same level of crosssectional stiffness. For example, according to the results presented in Figure 15, a cross-section area for 3+3 mm combination of 381×140 mm profile is more than 31% lower than for regular 10 mm plate, while the section modulus is more than 40% higher.
- The possibility of using high strength steel in such composite soil-steel structures was also investigated. The study revealed that in order to prevent local buckling thicker plates were necessary when higher yield strength steel was applied. The relationship is higher for the corrugation profiles with longer tangent length (see Figure 13). Therefore, minimal plate thickness to avoid local buckling was proposed for four specific and in practice widely used corrugation profiles for conventional and HSS.
- To validate and adjust numerical modelling results of this study, the performance of the laboratory test is necessary, and it is already planned in future work. In

addition, it is planned to perform investigation not only of axial compression of the corrugated plate, but also the combination of axial compression and bending moment.

Statement of the Use of Generative AI and AI-assisted Technologies in the Writing Process

The authors confirm that they did not use generative AI and AI-assisted technologies in the writing process.

Disclosure Statement

The authors confirm that they do not have any competing financial, professional, or personal interests from other parties.

REFERENCES

Andersson, A., & Karoumi, R. (2017). A soil-steel bridge under high-speed railways. *Archiwum Instytutu Inżynierii Lądowej*, *23*, 45–52. https://doi.org/10.21008/j.1897-4007.2017.23.04

Bareikis, N. (2024a). Parametric analysis of innovative corrugated profile of soil-steel composite bridge. *Ce/Papers*, *7*(3–4), 94–99. https://doi.org/10.1002/cepa.3072

Bareikis, N. (2024b). Rational steel mesh layout influence on plate utilization of large span corrugated steel structure. *Archives of Civil Engineering*, *70*(3), 561–578. https://doi.org/10.24425/ace.2024.151002

Bareikis, N. (2025). *High strength steel influence on sustainability of corrugated soil-steel composite bridge*, *IABSE Symposium: Environmentally Friendly Technologies and Structures: Focusing on Sustainable Approaches*, Tokyo, Japan, 807–814. https://doi.org/10.2749/tokyo.2025.0807

Beben, D. (2017). The role of backfill quality on corrugated steel plate culvert behaviour. *Baltic Journal of Road and Bridge Engineering*, *12*(1), 1–11. https://doi.org/10.3846/bjrbe.2017.01

Beben, D., & Manko, Z. (2010). Static tests on a soil-steel bridge structure with a relieving slab. *Structure and Infrastructure Engineering*, *6*(3), 329–346. https://doi.org/10.1080/15732470701511618

Beben, D., & Stryczek, A. (2016). Numerical analysis of corrugated steel plate bridge with reinforced concrete relieving slab. *Journal of Civil Engineering and Management*, *22*(5), 585–596. https://doi.org/10.3846/13923730.2014.914092

Bi, Z., & Yang, G. (2024). Buckling of corrugated steel plates under uniaxial compression. *Journal of Constructional Steel Research*, *223*, Article 109074. https://doi.org/10.1016/j.jcsr.2024.109074

Chen, T., Su, M., Pan, C., Zhang, L., & Wang, H. (2019). Local buckling of corrugated steel plates in buried structures. *Thin-Walled Structures*, *144*, Article 106348. https://doi.org/10.1016/j.tws.2019.106348

Cirulis, M., & Cirulis, M. (2017). Design and construction of railway snowfall protection structure on Baku-Tbilisi-Kars railway corridor. *Archiwum Instytutu Inżynierii Lądowej*, *23*, 81–90. https://doi.org/10.21008/j.1897-4007.2017.23.08

COMSOL AB. (2024). *COMSOL Multiphysics* (Version 6.3) [Software]. COMSOL Inc. https://www.comsol.com/

Cranston, P. G., Richie, M. C., & Vieira, L. C. M. (2016). Stability of buried corrugated metal pipe. *Proceedings of the Annual Stability Conference*, Structural Stability Research Council, Orlando, Florida. https://files.ssrcweb.org/proceedings/2016/stability-of-buried-corrugated-metal-pipe.pdf

Dou, C., Jiang, Z.-Q., Pi, Y.-L., & Guo, Y.-L. (2016). Elastic shear buckling of sinusoidally corrugated steel plate shear wall. *Engineering Structures*, *121*, 136–146. https://doi.org/10.1016/j.engstruct.2016.04.047

Du, G., Safi, M., Pettersson, L., & Karoumi, R. (2014). Life cycle assessment as a decision support tool for bridge procurement: environmental impact comparison among five bridge designs. *International Journal of Life Cycle Assessment*, *19*(12), 1948–1964. https://doi.org/10.1007/s11367-014-0797-z

Elshimi, T. M., Brachman, R. W. I., & Moore, I. D. (2014). Effect of truck position and multiple truck loading on response of long-span metal culverts. *Canadian Geotechnical Journal*, *51*(2), 196–207. https://doi.org/10.1139/cgj-2013-0176

Embaby, K., El Naggar, M. H., & El Sharnouby, M. (2022a). Performance of large-span arched soil–steel structures under soil loading. *Thin-Walled Structures*, *172*, Article 108884. https://doi.org/10.1016/j.tws.2022.108884

Embaby, K., Hesham El Naggar, M., & El Sharnouby, M. (2022b). Investigation of bevel-ended large-span soil-steel structures. *Engineering Structures*, *267*, Article 114658. https://doi.org/10.1016/j.engstruct.2022.114658

European Committee for Standardization. (2005). *EN 1993-1-1: Eurocode 3: Design of steel structures – Part 1-1: General rules and rules for buildings*. Brussels: CEN. https://www.phd.eng.br/wp-content/uploads/2015/12/en.1993.1.1.2005.pdf

Guo, T., & Sause, R. (2014). Analysis of local elastic shear buckling of trapezoidal corrugated steel webs. *Journal of Constructional Steel Research*, *102*, 59–71. https://doi.org/10.1016/j.jcsr.2014.06.006

Jeon, S., & Rigby, S. E. (2019). Design and numerical assessment of a rapid-construction corrugated steel-concrete-steel protective structure. *International Journal of Protective Structures*, *10*(4), 470–485. https://doi.org/10.1177/2041419619830703

Mahgoub, A., & El Naggar, H. (2021). Seismic design of metal arch culverts: design codes vs. full dynamic analysis. *Journal of Earthquake Engineering*, *25*(11), 2231–2268. https://doi.org/10.1080/13632469.2019.1625830

Maleska, T., & Beben, D. (2019). Numerical analysis of a soil-steel bridge during backfilling using various shell models. *Engineering Structures*, *196*, Article 109358. https://doi.org/10.1016/j.engstruct.2019.109358

Nakhostin, E., Kenny, S., & Sivathayalan, S. (2021). Numerical performance assessment of buried corrugated metal culvert subject to service load conditions. *Canadian Journal of Civil Engineering*, *48*(2), 99–114. https://doi.org/10.1139/cjce-2019-0316

Pettersson, L., Flener, E. B., & Sundquist, H. (2015). Design of soil-steel composite bridges. *Structural Engineering International: Journal of the International Association for Bridge and Structural Engineering (IABSE)*, *25*(2), 159–172. https://doi.org/10.2749/101686614X14043795570499

Pettersson, L., & Sundquist, H. (2014). *Design of soil steel composite bridges* (Report 112, 5th ed.). KTH Royal Institute of Technology. https://www.diva-portal.org/smash/get/diva2:761594/fulltext01.pdf

Piekarczuk, A., Malowany, K., Więch, P., Kujawińska, M., & Sulik, P. (2015). Stability and bearing capacity of arch-shaped corrugated shell elements: experimental and numerical study. *Bulletin of the Polish Academy of Sciences: Technical Sciences*, *63*(1), 113–123. https://doi.org/10.1515/bpasts-2015-0013

SolidWorks Corporation. (2024). *SOLIDWORKS* (Version 2024) [Software]. Dassault Systèmes. https://www.solidworks.com/

Sun, H. J., Guo, Y. L., Wen, C. B., Zuo, J. Q., Zhao, Q., & Liu, Z. G. (2023). The strength design of deeply buried circular corrugated steel arches with considering only soil radial restraining. *Thin-Walled Structures*, *183*, Article 110422. https://doi.org/10.1016/j.tws.2022.110422

Wadi, A., & Pettersson, L. (2017). Large-span soil steel composite bridges. *Archiwum Instytutu Inżynierii Lądowej*, *23*, 287–292. https://doi.org/10.21008/j.1897-4007.2017.23.26

Wadi, A., Pettersson, L., & Karoumi, R. (2018). FEM simulation of a full-scale loading-to-failure test of a corrugated steel culvert. *Steel and Composite Structures*, *27*(2), 217–227. https://doi.org/10.12989/scs.2018.27.2.217

Wadi, A., Pettersson, L., & Karoumi, R. (2020). On predicting the ultimate capacity of a large-span soil-steel composite bridge. *International Journal of Geosynthetics and Ground Engineering*, *6*(4). https://doi.org/10.1007/s40891-020-00232-z

Wang, T., Tan, L., Xie, S., & Ma, B. (2018). Development and applications of common utility tunnels in China. *Tunnelling and Underground Space Technology*, *76*, 92–106. https://doi.org/10.1016/j.tust.2018.03.006

Wysokowski, A. (2021). Influence of single-layer geotextile reinforcement on load capacity of buried steel box structure based on laboratory full-scale tests. *Thin-Walled Structures*, *159*, Article 107312. https://doi.org/10.1016/j.tws.2020.107312